Topoisomerase 1 dependent R-loop deficiency as a mechanism underlying oncogene-induced replication stress and genomic instability

Dan Sarni[1], Alon Shtrikman[1], Yifat S. Oren[1], and Batsheva Kerem[1,*]

[1]Department of Genetics, The Life Sciences Institute, The Hebrew University, Jerusalem 91904, Israel

[*]Corresponding Author

Corresponding Author:

Prof. Batsheva Kerem

Department of Genetics, The Life Science Institute

The Hebrew University, Jerusalem, Israel 91904

Email batshevak@savion.huji.ac.il

Fax 972-2-6584810

Key words: DNA replication, genomic instability, replication stress, oncogenes, Topoisomerase 1, R-loops.

Abstract

DNA replication is a complex process that is tightly regulated to ensure faithful genome duplication, and its perturbation leads to DNA damage and genomic instability. Oncogene expression triggers replicative stress that can lead to genetic instability, driving cancer progression. Thus, revealing the molecular basis for oncogene-induced replication stress is important for understanding of oncogenesis. Here we show that the activation of mutated HRAS leads to a non-canonical replication stress characterized by accelerated replication rate, inducing DNA damage. Mutated HRAS increases topoisomerase 1 (TOP1) expression, which leads to reduced levels of RNA-DNA hybrids (R-loops), driving fork acceleration and damage formation. Restoration of the perturbed replication either by restoration of TOP1 levels or directly by mild replication inhibition results in a dramatic reduction in DNA damage. The findings highlight the importance of TOP1 equilibrium in the regulation of R-loop homeostasis to ensure faithful DNA replication and genome integrity that when dysregulated can be a mechanism of oncogene-induced DNA damage.

Introduction

DNA replication is a complex process that is tightly regulated to ensure faithful duplication of the genome. Various factors are involved in regulating the different stages of replication, including origin licensing and firing, replication elongation rate and termination [1,2]. Under conditions that slow or even stall replication fork progression (defined as replication stress) dormant origins are activated to allow completion of DNA synthesis to maintain genome integrity [3,4]. However, insufficient compensation of the perturbed DNA replication may lead to genome instability [5,6]. Several factors are thought to lead to replication stress, among them are nucleotide deficiency, accumulation of RNA-DNA hybrids and DNA lesions [5,6], all of which result in perturbed replication dynamics and increase genomic instability.

Genomic instability is an important hallmark of cancer and a driver of tumorigenesis [7,8]. In recent years, aberrant activation of several oncogenes and tumor suppressor genes was found to induce replication stress leading to accumulation of DNA damage and an increased tumorigenecity potential [9–13]. This stress was characterized by slow replication rates, fork stalling, activation of dormant origins and even re-replication. Recently, however, several studies have found accelerated replication rates following alterations in expression of various genes [14–22]. These include down-regulation of mRNA biogenesis genes involved in mRNA processing and export [14,15], depletion of origin firing factors [17], inhibition of poly(ADP-ribose) polymerase (PARP) [19,20] and even overexpression of an oncogene, Spi-1 [21]. However, in only part of these studies accelerated replication was accompanied by DNA damage. Thus, it remains unclear whether the accelerated replication induces DNA damage per se. Similarly, the molecular mechanism/s underlying fork acceleration are largely unknown.

Here, we report an unexpected non-canonical form of oncogene-induced DNA damage caused by replication fork acceleration in pre-senescent cells. We show that activation of the mutated HRAS (RAS) oncogene induces an aberrant replication fork acceleration generating DNA damage and genomic instability. Mild replication inhibition restores the perturbed accelerated replication and reduces the DNA damage. We further investigate the molecular mechanism underlying this oncogene-induced replication acceleration and find that RAS activation leads to increased topoisomerase 1 (TOP1) expression, which leads to decreased RNA-DNA hybrids (R-loops). Restoration of the TOP1 level in RAS expressing cells restores R-loop levels and rescues the accelerated replication and DNA damage. Moreover, TOP1 overexpression by itself reduces R-loops, accelerates DNA replication and induces DNA damage. Finally, degradation of R-loops by overexpression of RNaseH1, also accelerates the replication rate and generates DNA damage. Altogether, these results highlight the important role of TOP1 in maintaining genome stability by controlling R-loop homeostasis, enabling tight regulation of DNA replication fork progression. Furthermore, the results reveal a novel mechanism of oncogene-induced DNA damage induced by aberrant replication fork acceleration.

Results

RAS expression induces replication acceleration in pre-senescent cells

RAS proteins are members of a GTP-binding protein family [23] which regulates numerous cellular processes including cell cycle progression [24]. Mutated RAS expression induces genomic instability [25–27] leading to senescence, a cell cycle arrest state serving as an antitumor barrier. However, cells escaping this proliferation inhibition drive tumorigenesis [28]. Therefore, we first investigated the effect of RAS on replication-induced genomic instability in pre-senescent cells. For this, immortalized human foreskin fibroblasts were retrovirally infected with an inducible ER:HRAS-G12V vector (referred to henceforth as RAS). RAS selective expression following 4-hydroxytamoxifen (4-OHT) supplementation was verified by Western blot (Fig. 1a). As expected, only cells infected with the RAS vector and treated with 4-OHT showed RAS expression compared with control cells; i.e., non-infected cells with RAS vector, whether treated or not with 4-OHT, or infected with RAS vector but not treated with 4-OHT (Fig. 1a). Following RAS activation cells entered a hyperproliferative phase, as indicated by increased population doubling and IdU incorporation already at day 2 (Supplementary Fig1. a-c). This was followed by a decline in proliferative potential until proliferation ceased by day 10, when cells entered senescence as indicated by reduced population doublings, reduced IdU incorporation and increased senescence associated β-gal activity (Supplementary Fig. 1a-e). Hence, the effect of RAS activation on replication dynamics and genome stability was investigated in pre-senescence RAS expressing cells up to 5 days following RAS induction.

We then analyzed the replication dynamics using the DNA combing approach, which enables replication analysis on single DNA molecules. Newly synthesized DNA extracted from

RAS-infected cells with (RAS) or without (control) 4-OHT treatment was labeled with IdU and CldU and detected by fluorescent antibodies (green and red, respectively) (Fig. 1b). The analysis was performed at two time points prior to senescence onset; at the hyperproliferative phase (day 2 post RAS activation) and at day 5 post RAS activation. First, we analyzed the effect of RAS activation on the DNA replication fork rate. The results showed a remarkable increase in the mean replication fork rate in both day 2 and day 5 following RAS activation (Fig. 1c). Similar results were obtained in an additional cell line of fetal human lung fibroblasts, WI-38 (Supplementary Fig. 2b).

Previous studies have shown that slow replication fork progression is correlated with an increased number of activated origins [3,4]. Therefore, we investigated origin activation in cells expressing RAS in which the replication rate is accelerated. Analysis of the mean replication fork distance showed a significant increase in the mean fork distance in both day 2 and day 5 following RAS activation (Fig. 1d). Similar results were obtained in WI-38 cells (Supplementary Fig. 2c). These results indicate that in pre-senescent RAS expressing cells there was a significant increase in the rate of replication fork progression along with a decrease in local origin activation.

Under replication stress which leads to fork stalling, asymmetrical progression of sister forks emanating from the same origin has been observed [2]. In order to further characterize the accelerated replication rate following RAS expression, we analyzed the symmetry of fork progression by comparing the progression of left and right outgoing sister replication forks. As previously suggested [2,10], the threshold for asymmetric progression of two forks was considered when the minimum to maximum sister forks ratio was < 0.75. The analysis showed that the vast majority of forks are symmetric in both day 2 and 5 following RAS expression as well as in

control cells (Fig. 1e, f). Similar results were obtained in WI-38 cells (Supplementary Fig. 2d, e), indicating no increase in fork stalling. Altogether, these results indicate a non-classical form of aberrant replication dynamics in pre-senescent RAS expressing cells, in which the replication fork speed is accelerated and fewer origins are activated. This aberrant accelerated replication was observed both when RAS-cells are hyperproliferating at day 2, and at day 5 while still proliferating but shortly before they senesce.

RAS expression leads to accelerated replication-induced DNA damage

Replication stress is known to induce DNA damage and thus DNA damage response pathways [29]. To determine whether RAS-induced replication fork acceleration causes replication-induced DNA damage we examined cellular DNA damage response markers known also to be induced under replication stress [30]. To do so, first we analyzed DNA damage formation as indicated by the co-localization of phosphorylated H2AX (γH2AX) and 53BP1 foci, after RAS activation. The analysis showed a significant increase in DNA damage in RAS-cells already at day 2 post RAS activation (Fig. 2a, b and Supplementary Fig. 3a), when aberrant acceleration of the DNA replication rate is already found (Fig. 1). Interestingly, the levels of DNA damage markers increased in RAS-cells over time (Fig. 2a, b and Supplementary Fig. 3a), implying that the accumulation of unrepaired damage may lead to cell cycle arrest, as previously suggested [9,12,28]. Next, we investigated whether the observed damage is associated with replication stress. Replication stress is known to induce DNA lesions which manifest as nuclear bodies of 53BP1 in the G1-phase of the next cell cycle [31]. Analysis of 53BP1 foci in G1-phase cells showed a significant increase in foci formation in pre-senescent RAS expressing cells compared with control cells (Fig. 2c, d). Similarly to 53BP1 foci analysis, we found in RAS expressing cells a significant increase in γH2AX, a DNA damage marker also induced upon replication stress

(Supplementary Fig. 3b, c) [30]. We then tested CHK1 activation, a hallmark of replication stress response [6], by analyzing its phosphorylation. As can be seen in Fig. 2e, a significant increase in CHK1 phosphorylation was found in RAS expressing cells compared with control cells. We also analyzed whether RAS activation leads to chromosomal fragility, since under replication stress conditions genomic instability is found preferentially at genomic regions known as fragile sites [32,33]. Metaphase spread analysis showed a significant increase in chromosomal fragility in RAS expressing cells compared with control cells (Fig. 2f, g), implying that the replication perturbation induced by RAS generates replication stress. Thus overall, these results suggest that the RAS-induced DNA damage is associated with the aberrant acceleration of DNA replication.

Previously, oncogene-induced replication stress was found to result from nucleotide insufficiency [10]. Viral and cellular oncogenes were shown to enforce cell proliferation without sufficient nucleotide biosynthesis to support normal replication [10]. Therefore, we investigated whether the replication-induced DNA damage following RAS expression could also result from a nucleotide deficiency. We analyzed 53BP1 foci in the G1-phase of RAS expressing cells grown in a regular medium or supplemented with exogenous nucleosides. The analysis showed no significant difference in replication-induced DNA damage foci (Supplementary Fig. 4a, b), indicating that DNA damage induced by fork acceleration was not the result of nucleotide insufficiency.

Reducing the accelerated replication fork progression rescues the DNA damage

We next investigated whether the replication fork acceleration could be the cause for DNA damage formation in RAS expressing pre-senescent cells. For this purpose, we slowed down the replication fork progression in RAS-cells and analyzed its effect on DNA damage formation. To

do so, we treated RAS-cells with hydroxyurea (HU), a known inhibitor of replication fork progression. HU inhibits the ribonucleotide reductase (RNR), thus reducing the deoxyribonucleotide pool, resulting in reduced replication fork progression in a dose-dependent manner [34–36]. Whereas high doses of HU (≥ 1mM) lead to fork arrest, low doses (≤ 0.1mM) decelerate replication fork progression [35,37]. Therefore, we used various relatively low HU concentrations and analyzed their effects on the replication dynamics. Cells expressing RAS for 5 days were treated with 0.001-0.1mM HU for 48 hours prior to the analysis, which allowed the cells to go through at least one cell cycle under inhibitory conditions (Fig. 3a). Flow cytometry analysis showed no significant change in the cell cycle progression, indicating that HU treatment did not arrest cell proliferation (Supplementary Fig. 5a, b). DNA combing analysis revealed that mild replication inhibition of RAS-cells with 0.01mM HU resulted in a dramatic replication deceleration compared with non-treated RAS-cells (Fig. 3b). The mean rate in these HU-treated RAS-cells showed no significant difference compared with control cells, indicating restoration of a normal replication fork rate (Fig. 3b). This HU concentration also led to a reduction in the fork distance in RAS expressing cells to the normal distance observed in the control cells (Fig. 3c). Finally, 0.01mM HU treatment did not induce sister fork asymmetry in RAS expressing cells, indicating that this low HU concentration did not induce fork stalling (Fig. 3d). Thus overall, these results indicate that mild replication inhibition rescued the perturbed DNA replication, resulting in the restoration of normal replication dynamics.

Next, we investigated whether the replication rate restoration affected RAS-induced DNA damage. For this purpose, cells were treated with 0.01mM HU for 48 hours prior to analysis of DNA damage by the immunofluorescence detection of co-localized DNA damage markers γH2AX and 53BP1. First, we analyzed the effect of this mild HU treatment in control

cells. The results showed no DNA damage induction (Supplementary Fig. 6a). We then analyzed the effect of mild HU treatment on RAS-cells. As seen in Figure 3f, 0.01mM HU treatment led to a significant decrease in the number of RAS-induced foci compared with non-treated RAS-cells (Fig. 3e, f). It is worth noting that the highest HU concentration (0.1mM) used caused dramatic replication fork slowing in RAS expressing cells even when compared with control cells (Fig. 3b). Accordingly, high HU treatment led to increased DNA damage formation compared with non-treated RAS-cells (Fig. 3e, f). A considerably lower dose of HU (0.001mM) had a limited, non-significant effect on the replication rate (Fig. 3b) and as expected had no significant effect on DNA damage formation compared with RAS expressing cells (Fig. 3e, f). Altogether these result indicate that the restoration of the accelerated replication rate dramatically reduced the DNA damage in RAS expressing cells.

We further investigated the effect of replication restoration on DNA damage by examining the effect of aphidicolin (APH), another replication inhibitor, which inhibits DNA polymerases α, δ, ε and decreases fork progression in a dose-dependent manner [38,39]. RAS expressing cells were treated with relatively low APH concentrations for 48 hours prior to replication dynamics and DNA damage analyses. Flow cytometry analysis showed no significant change in cell cycle progression, indicating that like HU, APH treatment did not arrest cell proliferation (Supplementary Fig. 5c, d). Co-localization analysis of γH2AX and 53BP1 foci revealed that a low dose of 0.01 μM APH significantly decreased the number of foci in RAS expressing cells compared with non-treated RAS-cells (Supplementary Fig. 6c, d), while it had no effect on the level of the damage markers in control cells (Supplementary Fig. 6a). Furthermore, similar to the effect of various HU concentrations, a very low dose of APH (0.001μM) did not have a significant effect on DNA damage formation in RAS-cells compared

with non-treated RAS expressing cells (Supplementary Fig. 6d); by contrast, a high dose of 0.1μM APH induced DNA damage formation (Supplementary Fig. 6d). Finally, we investigated whether the DNA damage rescue by the 0.01 μM APH treatment was associated with replication restoration. As expected, combing analysis showed restoration of the replication dynamics by the APH treatment (Supplementary Fig. 6e-g), suggesting that RAS-induced replication acceleration generates DNA damage.

Excess of Topoisomerase 1 levels causes an accelerated replication rate and DNA damage in RAS expressing cells

To explore the molecular mechanisms underlying the accelerated replication in RAS-cells, we examined the differences in gene expression after mutated RAS activation. For this purpose, we performed RNA-seq analysis on control and RAS expressing cells at two time points, at two- and four-days post-RAS activation, when cells are proliferating. Principal component analysis showed that the expression profiles of RAS-cells clustered together, and were distinguishable from the control cells (Supplementary Fig. 7a). After RAS activation >1,700 genes were differentially expressed, with an estimated false discovery rate (FDR) of < 5% and a fold change > 2-fold (Supplementary Fig. 7b). Gene Ontology (GO) annotation analysis of the upregulated genes following RAS activation (shared at both time points, 282 genes) showed enrichment for signaling and developmental processes (Supplementary Fig. 7c). Among the shared downregulated genes (568 genes) in RAS-cells, GO annotation analysis identified enrichment of anatomical and developmental processes in RAS expressing cells (Supplementary Fig. 7c). DNA replication was not found among the GO annotations significantly enriched after RAS activation. Therefore, we next focused on individual DNA replication annotated genes (GO:0006260) to identify specific differentially expressed genes in RAS as compared with control cells which

could lead to dysregulation of the replication process. Previously, deregulation of origin firing factors such as CDC7, ORC1, MCM4, MCM6, Treslin and MTBP have been shown to lead to an increased replication rate in various organisms [17–19]. However, our analysis showed no significant change in the expression level of any of these genes (Fig. 4a and Supplementary Table 1), suggesting that in our system the accelerated replication rate was not due to decreased origin usage. Analysis of replication annotated genes identified overexpression of topoisomerase 1 (TOP1) in RAS-cells (Fig. 4a and Supplementary Table 1). This increased level was further validated by Western blot and RT-qPCR (Fig .4b and Supplementary Fig. 8a).

TOP1 is an essential protein in mammalian cells that resolves the DNA torsional stress induced during replication and transcription by transiently nicking one strand of the DNA, thus allowing the second strand to pass through [40,41]. Reduced TOP1 activity by downregulation of TOP1 expression or functional inhibition was previously shown to dramatically reduce the replication fork rate and induce DNA damage [42]. Therefore, we set to investigate the potential role of TOP1 in the regulation of replication dynamics in RAS expressing cells. Specifically, we investigated the effect of excess TOP1 levels on replication dynamics and DNA damage. We first restored normal TOP1 level in RAS-cells by moderate downregulation of TOP1 using low concentrations of two independent siRNAs (Fig. 4c, d). After restoration of TOP1 levels, we examined the effect of restored TOP1 level on replication dynamics by DNA combing. The analysis showed that restoration of TOP1 to the normal expression level significantly reduced the replication rate in RAS-treated cells compared with non-treated RAS expressing cells (Fig. 4e), which was indistinguishable from the rate of the control cells, indicating complete restoration of a normal replication rate (Fig. 4e). TOP1 restoration also significantly reduced the fork distance in RAS-treated cells compared with non-treated RAS-cells (Fig. 4f), indicating restoration of the

replication dynamics (fork rate and origin firing). Finally, TOP1 restoration did not induce a significant increase in sister fork asymmetry, indicating that the mild siRNA downregulation did not induce fork stalling in RAS-cells (Fig. 4g).

Next, we investigated the effect of TOP1 restoration on RAS-induced DNA damage. We first downregulated TOP1 level in control cells and identified increased level of damage (Supplementary Fig. 8b, c), in agreement with previously published data [42], indicating that an aberrantly low level of TOP1 is deleterious to the cells. Next, we treated RAS-cells with siRNAs against TOP1, restoring normal expression level, and analyzed the DNA damage by immunofluorescence detection of γH2AX foci. The results showed a significant decrease in γH2AX levels subsequent to TOP1 siRNA treatment in RAS-cells compared with non-treated RAS-cells (Fig. 4h). This indicates that restoration of TOP1 level, to its normal level in control cells, rescues the DNA damage formation. Altogether, these results indicate that RAS-induced elevated level of TOP1 underlies the molecular mechanism of aberrant accelerated replication rate and genomic instability.

Reduced TOP1-dependent R-loops promote accelerated replication and DNA damage

To test our hypothesis that excess TOP1 accelerates replication rate leading to DNA damage formation, we overexpressed TOP1 in HEK 293 cell (Fig 5a) and analyzed its effect of replication dynamics using DNA combing. TOP1 overexpression significantly increased the mean replication rate compared with control cells (Fig 5b), and accordingly increased the fork distance (Fig 5c). Fork symmetry analysis revealed no increase in asymmetric fork progression following TOP1 overexpression (Fig. 5d), indicating that excess TOP1 expression accelerated DNA replication and did not cause fork stalling. Next, we measured DNA damage levels in

TOP1 overexpressing cells by immunofluorescence analysis of the DNA damage marker 53BP1. The analysis showed an increase in the mean number of foci following TOP1 overexpression compared with control cells (Fig 5e), supporting our findings that TOP1-dependent accelerated replication leads to DNA damage formation.

To explore how excess TOP1 accelerates DNA replication, we investigated the effect of elevated TOP1 on R-loop accumulation. R-loops are RNA-DNA hybrids formed during transcription and their aberrant accumulation may stall replication fork progression and thus lead to DNA damage [43]. Negative supercoiling, formed behind the transcribing RNA polymerase, promotes DNA strand separation which in turn increases the possibility of the nascent transcript to anneal to the DNA, and form an R-loop [43]. TOP1 relieves the negative supercoiled DNA behind the transcription machinery and thus prevents R-loop formation [43]. Indeed, TOP1 inhibition or down-regulation increases R-loop level [42]. Therefore, we posited that elevated TOP1 could promote accelerated replication by reducing the abundance of R-loops and therefore decrease potential obstacles to the replication machinery. Immunofluorescence analysis of RNA-DNA hybrids indeed showed a significant R-loop decrease in TOP1 overexpressing cells compared with control cells (Fig 5f), implying that reduced R-loop levels by increase TOP1 levels may promote accelerated replication rate.

Next, we explored the effect of excess TOP1 on R-loop levels in RAS expressing cells. Analysis of RNA-DNA hybrid levels showed a significant decrease in R-loops in RAS expressing cells for 2 and 5 days compared with control cells (Fig. 5g). We then analyzed the effect of TOP1 restoration in RAS-cell on R-loops, using two independent siRNAs against TOP1. The results showed that the siRNA treatment increased R-loop levels in RAS-cells compared with untreated RAS-cells (Fig. 5h). Notably, TOP1 restoration by siRNA increased R-

loop levels back to normal (Fig. 5h). These results indicate that restoration of TOP1 level in RAS-cells restores R-loop levels and rescues the accelerated replication rate and DNA damage.

Finally, we explored the direct effect of R-loop suppression on replication dynamics. For this purpose we overexpressed RNaseH1, which degrades R-loops, in HEK 293 cells (Fig. 6a). As expected RNaseH1 overexpression reduced the level of R-loops compared with control cells (Fig. 6b). RNaseH1 overexpression significantly accelerated the replication rate compared with control cells (Fig. 6c), and accordingly increased the mean fork distance (Fig. 6d). Fork symmetry analysis revealed no change following RNaseH1 overexpression (Fig. 6e). Lastly, immunofluorescence analysis of the DNA damage marker 53BP1, showed an increase in the mean number of foci following RNaseH1 overexpression compared with control cells (Fig. 6f). Taken together, the results indicate that suppressed R-loop levels promote replication fork acceleration and lead to the formation of DNA damage.

Discussion

Here, we report an unexpected form of oncogene-induced DNA damage caused by replication fork acceleration in pre-senescent cells expressing RAS. The molecular mechanism underlying this replication acceleration is increased TOP1 expression, which leads to reduced levels of R-loops (Supplementary Fig. 9). These results underscore the important role of TOP1 regulation of R-loop homeostasis in maintaining normal DNA replication and genome stability.

TOP1 is an essential protein for maintaining genome integrity. It relieves the topological stress arising during transcription and DNA replication, to enable proper progression of both machineries [41]. Inhibition or downregulation of TOP1 in cultured cells reduces the replication fork rate progression and induces DNA damage and genomic instability [42,44]. Furthermore, TOP1 knockout mice were shown to be embryonically lethal [45]. However, little is known about the effects of excess TOP1. A transient overexpression of TOP1 in cultured cells was reported to associate with activation of the DNA damage response [46]. Furthermore, a moderate increase in TOP1 levels was found in several cancers [47–49], thus, suggesting a possible contribution to genomic instability in cancer cells. Here we show that TOP1 is moderately overexpressed in RAS expressing cells, which leads to accelerated replication rate and DNA damage, as downregulation of TOP1 back to the control level restored replication dynamics and rescued the DNA damage (Fig 4). Furthermore, we show that TOP1 overexpression in non-oncogenic cells accelerated the replication rate and induced DNA damage (Fig. 5). Thus, these results highlight the deleterious nature of excess TOP1 and indicate that a tight regulation of TOP1 levels is essential for faithful replication and genome integrity.

The findings further indicated that the TOP1-induced accelerated replication and DNA damage were caused by reduced R-loop levels (Fig. 5 and Fig. 6). R-loops are transient RNA-

DNA hybrids formed during transcription. They were suggested to have a role in regulating gene expression and mediating transcription termination [43]. However, persistent R-loop accumulation is a major threat to genome integrity, as it introduces potential barriers to the replicating forks [43,50,51]. Indeed, head-on collisions between replication and transcription cause an accumulation of R-loops that activate the DNA damage response pathways [52]. During transcription, negative supercoiling is generated behind the RNA polymerase II, which facilitates the formation and accumulation of R-loops. TOP1 resolves this local negative supercoiling, thus suppressing the formation of R-loops [43]. Accordingly, reduced TOP1 activity was shown to increase R-loop-dependent replication stress [15,42]. Importantly, R-loop accumulation slows the replication rate and induces DNA damage [15,42,43,50,53]. Here we showed that an increase in the level of TOP1 leads to reduced R-loop accumulation both in RAS expressing cells and in non-oncogenic cells (Fig. 5f-h). Notably, suppression of R-loops by RNaseH1 overexpression accelerated the replication rate, decreased origin firing and generated DNA damage (Fig. 6). These results indicate a new role of TOP1-dependent R-loop formation in regulating DNA replication dynamics and genome stability. These findings broaden our understanding of the detrimental effects of unbalanced R-loop levels on DNA replication, as both excess and suboptimal levels perturb DNA replication and lead to DNA damage. Together, our results highlight the importance of TOP1 equilibrium in regulation of R-loop homeostasis to ensure faithful DNA replication and genome integrity. It should be noted that we cannot exclude the possibility that the effect of TOP1 on the rate of DNA replication may also result, in a non-mutually exclusive manner, from its role in resolving torsional stress ahead of the moving DNA replication machinery. Future investigation of the role of *in-vivo* excess TOP1 on the torsional stress ahead of replication forks is needed.

Recent studies have reported that inhibition of poly(ADP-ribose) polymerase (PARP) increases replication rate progression [19,20]. Interestingly, inhibition of PARP delocalized TOP1 from the nucleolus to the nucleoplasm [54] where replication of the bulk of the genome takes place. Thus, higher levels of TOP1 in the nucleoplasm may contribute to the observed accelerated replication rate after PARP inhibition, suggesting that elevated levels of TOP1 may be a general mechanism underlying replication acceleration.

Replication stress is usually characterized by fork slowing and even stalling; however other forms of replication perturbation have recently been reported, including replication fork acceleration associated with DNA damage formation [14–22]. Dysregulation of genes involved in mRNA biogenesis and export was reported to accelerate replication rate, potentially by impairing transcription elongation, thus reducing barriers to the replicating forks [14,15]. Overexpression of the interferon-stimulated gene 15, ISG15, was shown to accelerate replication rate via its interaction with the DNA helicase RECQ1 [22]. In addition, accelerated replication rate was reported following downregulation of several origin firing factors in various organisms [17,19]. Yet, our results showed no change following RAS activation in any of these genes (Fig. 4a and Supplementary Table 1) indicating that various mechanisms underlie the accelerated replication rate progression. Here we show that the aberrant accelerated fork progression found in RAS expressing cells leads to replication-induced DNA damage, as restoration of the perturbed replication dynamics by low HU/APH treatment rescued the damage (Fig. 3 and Supplementary Fig. 6). In order to test the possibility that the low HU/APH treatments activated the DDR, which might have contributed to the rescue of damage, we treated control cells with these low HU/APH concentrations and found no DDR activation (Supplementary Fig. 6a), as was previously shown by Koundrioukoff et al., [37]. Thus, indicating that in RAS-cells the DNA damage rescue by mild

replication inhibition is due to replication restoration. Altogether, our results indicate that accelerated replication rate generates DNA damage and shed light on the cascade of events generating genomic instability, from RAS expression that elevates TOP1 levels, which then reduces R-loops, resulting in the accelerated replication rate that causes DNA damage (Supplementary Fig. 9).

Our results also shed new light on a possible mechanism of oncogene-induced replication stress driving genomic instability. To date, replication stress induced by oncogenes has been characterized by replication fork slowing, which causes DNA damage [10,53,55–57]. This includes our previous study on cyclin E and HPV16 E6/E7, and work by others on Myc, RAS or CDC6. This damage was shown to result from either an insufficient nucleotide pool required to support normal DNA replication [10,55] or from accumulation of R-loops due to increased transcription [53]. Here we report a novel form of oncogene-induced DNA damage caused by accelerated replication. The DNA damage caused by fork acceleration could not result from increased R-loop accumulation since in RAS expressing cells, R-loop levels are reduced (Fig. 5g); nor could the damage result from nucleoside insufficiency, as exogenous nucleotide supply did not rescue the damage (Supplementary Fig. 4b). Our results therefore indicate that the damage induced by replication fork acceleration is mechanistically different from damage induced by fork slowing. It is worth noting that overexpression of the oncogene Spi-1 showed accelerated replication rate promoting genomic instability, however, without inducing DNA breakage [21]. Altogether, the molecular mechanism underlying accelerated replication-induced damage is still unknown; however, it is reasonable to speculate that increased replication rate may impair DNA polymerase fidelity, thus inducing DNA damage and genomic instability [58]. Further studies are required to investigate this hypothesis.

It is interesting to note that in recent studies of RAS-induced replication stress different results were obtained [12,53,56]. Di Micco et al., [12] found decreased origin firing and fork asymmetry following RAS activation in CHK2 deficient cells, however the replication rate was not reported. Mendoza et al., [56] reported a transient small but significant increase in the replication fork speed at the hyperproliferative phase of RAS expressing BJ cells, which was not accompanied with DNA damage possibly due to the small rate increase. This was followed by a decreased replication rate and increased DNA damage over time which was rescued by exogenous supply of dNTPs [56]. The authors suggested that hyperproliferation and increased fork rate can unbalance the nucleotide pool and cell metabolism, causing nucleotide insufficiency leading to the slowed replication rate and DNA damage [56]. Another study by Kotsantis et al., [53] reported that RAS overexpression in the same cells (BJ) led to an elevated expression of the general transcription factor TATA-box binding protein (TBP) at the hyperproliferative phase, leading to increased RNA synthesis, which together with R-loop accumulation results in replication fork slowing and DNA damage [53]. Importantly, in our system, however, RAS overexpression did not affect the TBP levels (Supplementary Table 1). Altogether, the different effects of RAS overexpression among the various studies may result from: (1) the level of RAS overexpression as RAS expression has a dose-dependent effect on cell proliferation and senescence onset [59], and (2) the use of different cellular systems (BJ, FSE and Wi-38) that may have accumulated genetic changes during cell culturing, leading to variations in gene expression patterns [60–62]. Despite the different effects of RAS in the various studies, the study by Kotsantis et al., and our study demonstrate the important role of balanced R-loop in maintaining genomic stability, as both low and high levels of R-loops promote genomic instability.

Altogether, here we reveal that TOP1 is a crucial factor for genome integrity, in that it tightly regulates replication dynamics. This further highlights the importance of TOP1-dependent R-loops homeostasis in replication regulation, as unbalanced levels impede replication dynamics and promote genomic instability. These results are also important for understanding early events leading to cancer development, as different mechanisms may underlie the oncogene-induced replication perturbation driving genomic instability. This sheds light on the complex nature of oncogene-induced replication stress, and suggests it should be taken into consideration when replication stress is considered as a therapeutic tool for cancer.

Methods

Cell Culture. Human foreskin fibroblasts, FSE-hTert cells, lung fibroblasts, WI38-hTert, and HEK-293 cells were grown in DMEM supplemented with 10% fetal bovine serum, 100,000 U l^{-1} penicillin and 100 mg l^{-1} streptomycin. ER:RAS activation was induced by supplementing the growth media with 200 μM of 4-hydroxytamoxifen (4-OHT). Nucleoside supplementation was achieved by supplementing the growth media with 50 μM of A, U, C and G each for 48 h prior to fixation. Aphidicolin and hydroxyurea treatments were performed in growth media with indicated concentrations for 48 h prior to fixation.

Plasmids. For ER:RAS infection, Phoenix retroviral packaging cells were transiently transfected with ER:RAS pLNC vector plasmids (kindly provided by Dr. J.C Acosta). Cells were infected three times with the Phoenix cell supernatant, containing replication-defective viruses. Infected FSE and WI38 cells were selected using 400 μg ml^{-1} G418 for the next 10 days. For TOP1-GFP transfection, HEK-293 cells were transiently transfected with pEGFP-TOP1 (kindly provided by Dr. Tasuku Honjo) or with a control GFP pBabe vector. Transfected cells were FACS sorted 24 h post transfection and 24 h later GFP positive cells were analyzed. For GFP-RNaseH1 transfection, HEK-293 cells were transiently transfected with pEGFP-RNaseH1 vector (kindly provided by Dr. Robert Crouch) or with a control GFP pBabe vector. Transfected cells were FACS sorted 24 h post transfection and 48 h later GFP positive cells were analyzed

Replication dynamics using DNA combing. Molecular combing is a process whereby single DNA molecules (hundreds of Kbs) are stretched on a silanized glass surface [63]. In general, unsynchronized cells were labeled for 30 min by medium containing 100 μM of the thymidine analog iododeoxyuridine (IdU). At the end of the first labeling period, the cells were washed twice with a warm medium and pulse labeled once more for 30 min with a medium containing

100 μM chlorodepxyuridine (CldU) and then washed with cold PBS and harvested. Genomic DNA was extracted, combed and analyzed as previously described [64]. The primary antibody for fluorescence detection of IdU was mouse anti-BrdU (Becton Dickinson), and the secondary antibody was goat anti-mouse Alexa Fluor 488 (Invitrogen). The primary antibody for fluorescence detection of CldU was rat anti-CldU (Novus Biologicals). The secondary antibody was goat anti-rat Alexa Fluor 594 (Invitrogen). The primary antibody for fluorescence detection of ssDNA was mouse anti-ssDNA (Millipore). The secondary antibody was donkey anti-mouse Alexa Fluor 647 (Invitrogen). The length of the replication signals and the fork distances were measured in micrometers and converted to kilo bases according to a constant and sequence-independent stretching factor (1μm = 2kb), as previously reported [64]. Images were analyzed double blindly using Fiji [65].

Immunofluorescence staining. Cells were fixed in 4% formaldehyde/PBS for 10 min, permeabilized with 0.5% Triton/PBS for 10 min, and blocked with 10% fetal bovine serum/PBS for 1-3 h. The primary antibodies used were mouse anti-phosphorylated H2AX (Upstate Biotechnology, 1:100), rabbit anti-53BP1 (Bethyl Laborartories, 1:100), mouse anti-cyclin A2 (Abcam, 1:100) and mouse anti-BrdU (Becton Dickinson, 1:25). For RNA-DNA hybrid detection, cells were washed with cold PBS and fixed with 100% ice-cold methanol for 7 min and incubated overnight in blocking solution 3% BSA/PBS. S9.6 antibody (kindly provided by Dr. Rachel Eiges) was used, 1:500. Secondary antibodies added were anti–mouse Alexa Fluor 488 (Invitrogen), anti-rabbit Alexa Fluor 488 (Invitrogen), anti-mouse Alexa Fluor 555 (Invitrogen). DNA was counterstained with mounting medium for fluorescence with DAPI (Vector Laboratories). For focus information analysis images were taken with the FV-1200 confocal microscope (Olympus, Japan), with a 60X/1.42 oil immersion objective. Multiple dyes

sequential scanning mode was used in order to avoid emission bleed-through. For focus and fluorescent intensity analysis the Hermes WiScan system (Idea Bio-Medical, Israel) was used. All images were analyzed double blindly using Fiji [65].

Metaphase chromosome preparation and fragile site analysis. Cells were treated with 100 ng ml^{-1} colcemid (Invitrogen) for 15–40 min, collected by trypsinization, treated with hypotonic solution at 37 □C for 30 min and fixed with multiple changes of methanol:acetic acid 3:1. Fixed cells were kept at -20°c until analysis. For analysis of total gaps and breaks chromosomes were stained with propidium-iodide and analyzed double blindly using Fiji [65].

Western blot analysis. 8-12% polyacrylamide gels were used for protein separation and detection. The gels were transferred to a nitrocellulose membrane, and antibody hybridization and chemiluminescence (ECL) were performed according to standard procedures. The primary antibodies used in these analyses were rabbit anti-H-RAS (Santa Cruz, 1:1,000), mouse anti-CHK1 (Cell signaling, 1:500), rabbit anti-phosphorylated CHK1 (Cell Signaling, 1:200), rabbit anti-GAPDH (Cell Signaling, 1:1,000), mouse anti-β-catenin (BD-Biosciences, 1:2,500), mouse anti-Tubulin (Sigma, 1:50,000), rabbit anti-TOP1 (Abcam, 1:10,000)), and rabbit anti-RNaseH1 (Abcam, 1:1,000). HRP-conjugated anti-rabbit and anti-mouse secondary antibodies was obtained from Jackson Immunoresearch Laboratories (711-035-152, 1:5,000).

Population doublings. Cells were grown in media as indicated in the 'Cell Culture' section. Initial seeding concentration of cells was 10,000 per well. Cells were trypsinized and counted. Population doublings (PD) was measured according to the following formula:

$$PD = [log\ (Xe\ \div Xb)\ \div log\ (2)]$$

Xb is the number of cells at the beginning of incubation and Xe is the number of cell at the final count [66].

RNA sequencing analysis. Sequencing libraries were prepared using the Illumina TruSeq mRNA kit, and sequenced (60 bp, single reads) on a single lane of Illumina HiSeq 2500 V4 instrument, to a depth of ~27 million reads per sample. Reads were aligned to the hg19 genome (UCSC, downloaded from iGenomes) using TopHat (v2.0.10) [67]. HTSeq-count (version 0.6.1p1) [68] was used to count reads on gene exons (UCSC Annotation from March 9, 2012). Differential expression analysis was performed using DESeq2 (1.6.3) [69] with betaPrior set to False. Gene set enrichment analysis was performed using WebGestalt [70].

RNA analysis. Total RNA was extracted using the RNeasy Mini Kit extraction kit (QIAGEN). RNA-less and reverse transcriptase-less reactions were used as controls. Complementary DNA (cDNA) synthesis was performed using the High Capacity cDNA Reverse Transcription kit (Applied Biosystems). Real-time PCR was subsequently performed in ABI 7500 using a Power SYBR green PCR master Mix (Applied Biosystems). The expression level was normalized to the transcript levels of GAPDH. Specific primers for these PCRs were designed using the Primer Express software:
GAPDH: Fwd, TGAGCTTGACAAAGTGGTCG; Rev, GGCTCTCCAGAACATCATCC,
POLR2A: Fwd, TGCGCA CCATCAAGAGAGTC; Rev, CTCCGTCACAGACATTCGCTT,
TOP1: Fwd, CCCTGTACTTCATCGACAAGC; Rev, CCACAGTGTCCGCTGTTTC.

siRNA. siRNA against TOP1 (TOP1-1: 5'-GCACAUCAAUCUACACCCA-3' and TOP1-2: 5'-CGAAGAAGGUAGUAGAGUC-3') and a control, non-targeting siRNA (Ctrl: 5'-UGGUUUACAUGUCGACUAA-3') were purchased from Dharmacon. Cells were transfected

with 40nM control siRNA and 20nM siRNA against TOP1, using oligofectamine (Thermo-Fisher). Cells were analyzed 48 hours after transfection.

Cell cycle analysis. Cells were harvested and the pellet resuspended in 0.5ml cold PBS and fixed in 4.5ml 100% chilled methanol and kept at -20ºC. Prior to FACS analysis, methanol residues were washed and cells were resuspended in PBS containing 0.2µg/µl RNase for 30 min. Cells were stained with 50µg/ml propidium iodide and the DNA content was analyzed by flow cytometry (BD FACSAria III).

Statistical analysis. All data analysis was performed using Excel, GraphPad Prism 8.3.0 for Windows, GraphPad Software, La Jolla California USA (www.graphpad.com) or R project for Statistical Computing (htpp://www.r-project.com). For comparisons of replication dynamics (relevant to Fig. 1,3,4,5,6 and Supplementary Fig. 2,6), Immunofluorescence staining (relevant to Fig. 2,3,4,5,6 and Supplementary Fig. 3,4,6,8), metaphase spreads analyses (relevant to Fig. 2) and SA-β gal activity (relevant to Supplementary Fig. 1) one-way ANOVA and Mann-Whitney rank sum test were performed, as indicated. Numbers of repeats are indicated in the figure legends.

Data availability. The authors declare that all the data supporting the findings of this study are available within the article and its Supplementary Information files and from the corresponding authors upon reasonable request.

Acknowledgements

This research was supported by grants from the Israel Science Foundation (grant No. 176/11), the Israeli Centers of Research Excellence (I-CORE), Gene Regulation in Complex Human Disease, Center No 41/11/", and by the ISF-NSFC joint program (grant No. 2535/16). The authors thank Dr. Naomi Melamed-Book for her assistants in confocal microscopy. The authors thank the Mantoux Bioinformatics institute of the Nancy and Stephen Grand Israel National Center for Personalized Medicine, Weizmann Institute of Science, for assistant in deep sequencing and bioinformatics analysis. The authors thank the members of the Kerem lab for thoughtful discussions and advice.

Author contributions

D.S contributed to conception and design, performed experiments, collection and assembly of data, data analysis and interpretation and manuscript writing; A.S performed and contributed to the experimental analyses, data interpretation and graphical abstract; Y.S.O performed and contributed to the experimental analyses and data interpretation; B.K contributed to conception and design, financial support, data analysis and interpretation, manuscript writing and final approval of the manuscript.

Competing financial interests: The authors declare no competing financial interests.

Figure legends

Fig. 1. RAS expression leads to increased replication rate and fork distance. (**a**) Protein levels of HRAS and GAPDH in FSE-hTert cells with (+) or without (-) ER:RAS infection and 4-OHT treatment as indicated. (**b**) Top: a scheme of the protocol. Cells infected with ER:RAS with (RAS) or without (Control) 4-OHT treatment were pulse-labeled with two thymidine analogs (IdU then CldU) for 30 min each. DNA combing was performed 2 or 5 days after RAS induction (4-OHT treatment). Bottom: representative images of labeled DNA fibers. (**c**) Dot plots of individual replication fork rates (kb/min) in control and RAS expressing cells for 2 or 5 days; at least 240 fibers per condition were analyzed. (**d**) Dot plots of individual fork distances (kb) in control and RAS expressing cells for 2 or 5 days; at least 110 fibers per condition were analyzed. (**e**) Dot plots of sister fork symmetry ratios in control and RAS expressing cells for 2 or 5 days; at least 100 fibers per condition were analyzed. Fork symmetry is expressed as the ratio of the shorter to the longer distance covered during the IdU pulse, for each pair of sister replication forks. Dashed green line indicates asymmetry ratio threshold. (**c-e**) Red lines indicate medians, Means are indicated. (**f**) Scatter plots of the replication rates (kb/min) of right- and left-moving sister forks during IdU pulse. The center areas delimited with red lines contain sister forks with less than 25% difference. The percentages of symmetric forks are indicated at the top left corner of the plots, control and RAS expressing cells for 2 or 5 days. (**c-f**) Data for RAS day 2 are the summary of 2 independent experiments; data for RAS day 5 are the summary of 4 independent experiments. Mann-Whitney rank-sum test, ns – non-significant; * $P < 0.05$, ** $P < 0.01$, **** $P < 0.0001$.

Fig. 2. RAS expression leads to accelerated replication-induced DNA damage in pre-senescent cells. (**a,b**) Co-localization of γH2AX (red) and 53BP1 (green) foci in ER:RAS FSE-hTert cells with (+) or without (-) 4-OHT treatment for the indicated time points (days). Representative images (**a**), quantification of the mean co-localized γH2AX and 53BP1 foci per cell (**b**); number of analyzed cells from left to right: n = 399, 384, 467, 762, 704, 501, respectively. Data are the summary of three independent experiments, means ± s.e.m are shown. *P* values calculated compared to ER:RAS FSE-hTert cells without 4-OHT (-) treatment (Ctrl) by one-way ANOVA. (**c,d**) 53BP1 foci in G1-phase (cyclin A negative cells) in FSE-hTert cells with (+) or without (-) ER:RAS infection and 4-OHT treatment as indicated. Representative images of 53BP1 foci (green) in cyclin A (red) negative cells and DAPI staining (blue) (**c**), quantification of the percent of cells with indicated number of foci per nucleus (**d**); number of analyzed nuclei from left to right: n = 93, 126, 133, 87, respectively. *P* values calculated compared to ER:RAS FSE-hTert cells treated with 4-OHT (RAS). Data are representative of three independent experiments with similar results. (**e**) Protein levels of phosphorylated Chk1 ser345, Chk1 and β-catenin in FSE-hTert cells with (+) or without (-) ER:RAS infection and 4-OHT treatment as indicated. (**f**) A representative image of a metaphase spread in FSE-hTert RAS cells, the box at the bottom right corner shows magnification of the chromosomes in the selected smaller box; red arrow indicates a break. (**g**) Quantification of chromosomal aberrations detected in metaphase spreads of ER:RAS FSE-hTert cells treated with 4-OHT for 4 days (RAS, n = 120) or without 4-OHT treatment (Control, n = 155). The results are the average number of chromosomal aberrations from two independent experiments, means ± s.e.m are shown. Mann Whitney rank-sum test, * $P < 0.05$, ** $P < 0.01$, *** $P < 0.001$; **** $P < 0.0001$. Scale bars, 10 μm.

Fig. 3. Mild replication inhibition restores normal replication dynamics and rescues DNA damage. (**a**) Scheme of the protocol. Cells infected with ER:RAS without 4-OHT treatment (Control) were cultured for 120h. Cells treated with 4-OHT (RAS) were cultured for 120h, with (+) or without (-) HU treatment for the last 48h, followed by DNA combing or immunofluorescence (IF). (**b-d**) DNA combing analysis of FSE-hTert cells with (+) or without (-) 4-OHT and HU treatments as indicated. Individual replication fork rates (kb/min); at least 300 fibers per condition were analyzed (**b**). Individual fork distances (kb); at least 150 forks per condition were analyzed (**c**). Individual sister fork symmetry ratios; at least 110 forks per condition were analyzed (**d**). Means are indicated; Red lines indicate medians. *P* values calculated compared to FSE-hTert cells without 4-OHT treatment (Control) by one-way ANOVA. Data are the summary of two independent experiments. (**d**) Dashed green line indicates asymmetry ratio threshold. (**e,f**) Co-localization of γH2AX (red) and 53BP1 (green) foci in ER:RAS FSE-hTert cells with (+) or without (-) 4-OHT and HU treatments as indicated. Representative images (**e**), quantification of the percent of cells with indicated number of foci per nucleus (**f**); number of analyzed nuclei from left to right: n = 286, 336, 194, 273, 276, respectively. Data are representative of two independent experiments with similar results. *P* values calculated compared to ER:RAS FSE-hTert cells treated with 4-OHT (+) but without HU (-) (RAS) by Mann Whitney rank-sum test. ns – non-significant; * $P < 0.05$, ** $P < 0.01$, *** $P < 0.001$, **** $P < 0.0001$. Scale bars, 10 μm.

Fig. 4. Increased TOP1 expression causes accelerated DNA replication and DNA damage. (**a**) Expressed DNA replication annotated genes (GO:0006260, n=258) ranked according to the RAS/Control fold change ratio. Light blue - genes previously associated with accelerated replication rate; red - TOP1. (**b**) Protein levels of TOP1 and Tubulin in FSE-hTert cells with (+) or without (-) ER:RAS infection and 4-OHT treatment as indicated. (**c**) Protein levels of TOP1 and GAPDH in ER:RAS infected FSE cells with (RAS) or without (Ctrl) 4-OHT treatment, and treated with two independent siRNAs against TOP1 (siTOP1-1 and siTOP1-2) or non-targeting siRNA (siCtrl), as indicated. (**d**) ER:RAS FSE hTert cells treated with 4-OHT (RAS) were treated with two independent siRNAs against TOP1 (siTOP1-1 and siTOP1-2) and non-targeting siRNA (siCtrl). Levels of TOP1 were measured by RT-qPCR and normalized to GAPDH. The values are averaged fold change (mean ± s.e.m, n = 2) relative to ER:RAS FSE hTert cells without 4-OHT treatment. (**e-g**) DNA combing analysis of ER:RAS FSE-hTert cells with (+) or without (-) 4-OHT and siRNA treatments as indicated. Individual replication fork rates (kb/min); at least 270 fibers per condition were analyzed (**e**). Individual fork distances (kb); at least 140 forks per condition were analyzed (**f**). Individual sister fork symmetry ratios; at least 125 forks per condition were analyzed (**g**). Means are indicated; Red lines indicate medians. *P* values calculated by one-way ANOVA. Data are the summary of two independent experiments. (**g**) Dashed green line indicates asymmetry ratio threshold. (**h**) Percent of cells with the indicated number of γH2AX foci in ER:RAS FSE-hTert cells with (+) or without (-) 4-OHT and siRNA treatments as indicated; number of analyzed nuclei from left to right: n = 2644, 1021, 2223, 3367, respectively. *P* values calculated compared to ER:RAS FSE-hTert cells treated with 4-OHT and siCtrl (RAS), Mann Whitney rank-sum test. Data are representative of three independent experiments. ns – non-significant; *** $P < 0.001$, **** $P < 0.0001$.

Fig 5. TOP1 overexpression reduces R-loop level leading to accelerated DNA replication and damage. (**a**) Protein levels of endogenous TOP1 (TOP1), ectopic TOP1 (TOP1-GFP) and GAPDH in HEK-293 cells transfected with a control GFP vector (Ctrl) or with TOP1-GFP (TOP1), as indicated (**b**-**d**) DNA combing analysis of HEK-293 cells as indicated in **a**. Individual replication fork rates (kb/min) ; at least 400 fibers per condition were analyzed (**b**). Individual fork distances (kb); at least 180 forks per condition were analyzed (**c**). Individual sister fork symmetry ratios; at least 180 forks per condition were analyzed (**d**). Means are indicated; Red lines indicate medians. *P* values calculated by Mann Whitney rank-sum test. Data are the summary of two independent experiments. Dashed green line indicates asymmetry ratio threshold (**d**). (**e**) 53BP1 foci in HEK-293 cells as indicated in **a**. Left: Representative images of 53BP1 (green) foci and DAPI (blue) staining. Right: Quantification of the percent of cell with indicated number of 53BP1 foci. At least 300 nuclei were analyzed. Data are representative of two independent experiments. (**f**) RNA-DNA hybrids in HEK-293 cells as indicated in **a**. Left: Representative images of RNA-DNA specific antibody (S9.6, red) and DAPI (blue) staining. Right: Dot plot of mean nuclear fluorescence intensity of RNA-DNA hybrid specific antibody (S9.6) in individual nuclei. At least 600 nuclei were analyzed. Data are summary of two independent experiments. (**g**) RNA-DNA hybrids in ER:RAS FSE hTert cells with (RAS) or without (Ctrl) 4-OHT treatment. Left: representative images of RNA-DNA specific antibody (S9.6, red) and DAPI (blue) staining. Right: Dot plots of mean nuclear fluorescence intensity of RNA-DNA hybrids (S9.6 antibody) in individual nuclei in control (Ctrl) and RAS expressing cells for 2 or 5 days. (**h**) Dot plot of mean nuclear fluorescence intensity of RNA-DNA hybrid specific antibody (S9.6) in individual nuclei in ER:RAS FSE hTert cells with (RAS) or without

(Ctrl) 4-OHT treatment, and siRNA treatments as indicated. * $P < 0.05$; ** $P < 0.01$; **** $P < 0.0001$. Scale bars, 10 μm.

Fig 6. Reduced R-loops causes accelerated DNA replication rate and DNA damage. (**a**) Protein levels of GFP-RNaseH1 and GAPDH in HEK-293 cells transfected with a control GFP plasmid (Ctrl) or with GFP-RNaseH1 plasmid (RNaseH1). (**b**) RNA-DNA hybrids in HEK-293 cells transfected with a control GFP plasmid (Ctrl) or with a GFP-RNaseH1 plasmid (RNaseH1). Left: Representative images of RNA-DNA specific antibody (S9.6, red) and DAPI (blue) staining. Right: Dot plot of mean nuclear fluorescence intensity of RNA-DNA hybrid specific antibody (S9.6) in individual nuclei of Ctrl (n = 291) and RNaseH1 (n = 439). Data are the summary of two independent experiments. (**c-e**) DNA combing analysis of HEK-293 cells transfected with a control GFP plasmid (Ctrl) or with GFP-RNaseH1 plasmid (RNaseH1). Individual replication fork rates (kb/min) in Ctrl and RNaseH1 cells; at least 250 fibers per condition were analyzed (**c**). Individual fork distances (kb) in Ctrl and RNaseH1 cells; at least 130 fibers per condition were analyzed (**d**). Individual sister fork symmetry ratios in Ctrl and RNaseH1 cells; at least 90 fibers per condition were analyzed (**e**). (**c-e**) Means are indicated; Red lines indicate medians. *P* values calculated by Mann Whitney rank-sum test. Data are the summary of two independent experiment. Dashed green line indicates asymmetry ratio threshold (**e**). (**f**) 53BP1 foci in HEK-293 cells transfected with a control GFP plasmid (Ctrl) or with GFP-RNaseH1 plasmid (RNaseH1). Left: Representative images of 53BP1 (green) foci and DAPI (blue) staining. Right: quantification of the percent of cell with indicated number of 53BP1 foci in Ctrl (n = 1120) and RNaseH1 (n = 1111). Data are the summary of two independent experiments. ns – non-significant; **** $P < 0.0001$. Scale bars, 10 μm.

Supplementary legends

Supplementary Fig. 1. Related to Fig. 1. RAS expression induces senescence. (**a**) Quantification of population doublings at the indicated time points in: FSE-hTert cells (hTert, n = 4); FSE-hTert with 4-OHT treatment (hTert + 4-OHT, n = 2); FSE-hTert with ER:RAS infection but without 4-OHT treatment (ER:RAS, n = 4); FSE-hTert with ER:RAS infection and 4-OHT treatment (ER:RAS + 4-OHT, n = 4). n represents the number of independent experiments; data are mean ± s.e.m. (**b**) Representative images of IdU (green) and DAPI staining (blue) in RAS expressing cells at the indicated time points. (**c**) Quantification of the percent of control (Ctrl) and RAS nuclei positive for IdU incorporation at the indicated time points (days post RAS activation). Data are mean ± s.e.m from two independent experiments. (**d**) Representative images of senescence associated β-gal activity, positive cells are stained blue. (**e**) Quantification of senescence associated β-gal activity in FSE-hTert cells with (+) or without (-) ER:RAS infection and 4-OHT treatment at the indicated time points (days). Data are the summary of two independent experiments. *P* values calculated compared to FSE-hTert cells without ER:RAS infection nor 4-OHT treatment. Mann Whitney rank-sum test, ns - nonsignificant; **** $P < 0.0001$. Scale bars, 20 μm.

Supplementary Fig. 2. Related to Fig 1. RAS expression leads to increased replication rate and fork distance in WI38 cells. (**a**) Protein levels of HRAS and GAPDH in WI38-hTert cells with (+) or without (-) ER:RAS infection and 4-OHT treatment as indicated. (**b**) Dot plots of individual replication fork rates (kb/min) in WI38-hTert infected with ER:RAS without (Control) or with (RAS) 4-OHT treatment for 5 days; at least 600 fibers per condition were analyzed. (**c**)

Dot plots of individual fork distances (kb) in Control and RAS cells; at least 260 fibers per condition were analyzed. (**d**) Dot plots of sister fork symmetry ratios in Control and RAS cells; at least 230 fibers per condition were analyzed. Dashed green line indicate asymmetry ratio threshold. (**b-d)** Red lines indicate medians, means are indicated. (**e**) Scatter plots of the replication rates (kb/min) of right- and left-moving sister forks during IdU pulse. The center areas delimited with red lines contain sister forks with less than 25% difference. The percentages of symmetric forks are indicated at the top left corner of the plots. (**b-e**) Data are the summary of two independent experiments, Mann-Whitney rank-sum test, ns - nonsignificant; **** $P < 0.0001$.

Supplementary Fig 3. Related to Fig 2. RAS leads to accelerated replication-induced DNA damage in pre-senescent cells. (**a**) Percent of cells with indicated number of co-localized γH2AX and 53BP1 foci in ER:RAS FSE-hTert cells with (RAS) or without (Ctrl) 4-OHT treatment for the indicated time points (days). Data are the summary of three independent experiments. *P* values calculated compared to ER:RAS FSE-hTert cells without 4-OHT (-) treatment (Ctrl). (**b**) Representative images of γH2AX foci (green) and DAPI staining (blue) in FSE-hTert cells with (+) or without (-) ER:RAS infection and 4-OHT treatment as indicated. (**c**) Percent of cells with the indicated number of γH2AX foci in FSE-hTert cells with (+) or without (-) ER:RAS infection and 4-OHT treatment as indicated; number of analyzed nuclei from left to right: n = 145, 148, 144, 94, respectively. *P* values calculated compared to ER:RAS FSE-hTert cells treated with 4-OHT (RAS). Data are representative of two independent experiments with similar results.

Supplementary Fig. 4. Related to Fig 2. DNA damage induced by RAS expression is not a result of nucleotide insufficiency. (**a**) Representative images of 53BP1 foci (green) in cyclin A (red) negative cells and DAPI staining (blue) in FSE-hTert cells infected with ER:RAS and treated with 4-OHT for 5 days with (+) or without (-) nucleoside supplementation (dNTPs). (**b**) Quantification of the mean 53BP1 foci in cyclin A negative ER:RAS FSE-hTert cells with 4-OHT treatment for 5 days, with exogenously supplementation of nucleosides (n = 273) or without (n = 293). Results are the summary of two independent experiments. Means ± s.e.m are shown. Mann-Whitney rank-sum test, ns - nonsignificant. Scale bars, 20 μm.

Supplementary Fig. 5. Related to Fig 3. Mild replication inhibition does not affect cell cycle progression. (a) Flow cytometry analysis of ER:RAS FSE-hTet cells treated with 4-OHT and HU as indicated. (**b**) Quantification of data presented in (**a**). (**c**) Flow cytometry analysis of ER:RAS FSE-hTet cells treated with 4-OHT and APH as indicated. (**d)** Quantification of data presented in (**c**). Data are representative of two independent experiments.

Supplementary Fig. 6. Related to Fig 3. Mild replication inhibition restores normal replication dynamics and rescues DNA damage. (**a**) Percent of cells with the indicated number of co-localized γH2AX and 53BP1 foci in ER:RAS infected FSE-hTert cells without 4-OHT treatment (control), treated with HU and APH as indicated. Cells treated with 0.2μM APH as a control, using a high APH concentration that generates DNA damage. Data are the summary of two independent experiments. (**b**) Scheme of the protocol. Cells infected with ER:RAS without

4-OHT treatment (control) were cultured for 120h. Cells treated with 4-OHT (RAS) were cultured for 120h, with (+) or without (-) aphidicolin (APH) treatment for the last 48h, followed by DNA combing or immunofluorescence (IF). (**c,d**) Co-localization of γH2AX (red) and 53BP1 (green) foci in ER:RAS FSE-hTert cells with (+) or without (-) 4-OHT and APH treatment at the indicated concentrations. Representative images (**c**), quantification of the percent of cells with indicated number of foci (**d**); number of analyzed nuclei from left to right: n = 142, 137, 142, 164, 141, respectively. Data are representative of two independent experiments with similar results. *P* values calculated compared to ER:RAS FSE-hTert cells treated with 4-OHT (+) but without APH (-) (RAS). (**e-g**) DNA combing analysis of ER:RAS FSE-hTert cells with (+) or without (-) 4-OHT and APH treatments as indicated. Individual replication fork rates (kb/min); at least 270 fibers per condition were analyzed (**e**). Individual fork distances (kb); at least 130 forks per condition were analyzed (**f**). Individual sister fork symmetry ratios; at least 110 forks per condition were analyzed (**g**). Red lines indicate medians. (**g**) Dashed green line indicates asymmetry ratio threshold. Data are the summary of two independent experiments. *P* values calculated by one-way ANOVA (**e-g**) and by Mann Whitney rank-sum test (**d**), ns - nonsignificant; * *P* value < 0.05, ** *P* < 0.01, *** *P* < 0.001, **** *P* < 0.0001. Scale bars, 10 μm.

Supplementary Fig. 7. Related to Fig 4. RNA-seq analysis of RAS expressing cells. (**a**) Principal component analysis (PCA) plot of gene expression data showing the 1st and 2nd principal components for control (red), RAS day 2 (green) and RAS day 4 (blue). (**b**) Hierarchical clustering heat map for differentially expressed genes (DEGs) between RAS expressing cells for 2 or 4 days (RAS day 2 and RAS day 4, respectively) and control cells. The

Z-score centered log2-transformed gene in each sample is presented using a color scale. Three independent biological replicates are presented (1-3). (**c**) Top: Venn diagrams of upregulated (UP) or downregulated (DOWN) DEGs after RAS activation, showing overlap between RAS day 2 and RAS day 4. Bottom: Gene ontology (GO) term analyses of DEGs shared by RAS day 2 and RAS day 4. The top 10 enriched biological processes are shown.

Supplementary Fig 8. Related to Fig. 4. Elevated TOP1 expression in RAS expressing cells. (**a**) RNA-seq and RT-qPCR analyses of TOP1 in ER:RAS FSE-hTert cells treated with 4-OHT for 2 and 4 days (RAS day 2 and RAS day 4, respectively) relative to non-treated cells. For the RT-qPCR analysis, the values were normalized to those of RNA polymerase II and are the average fold change (mean ± s.e.m, n = 3). (**b**) Protein levels of TOP1 and GAPDH in ER:RAS FSE-hTert cells without 4-OHT treatment (Control), treated with two independent siRNAs against TOP1 (siTOP1-1 and siTOP1-2) and non-targeting siRNA (siCtrl). (**c**) Percent of cells with indicated number of co-localized γH2AX and 53BP1 foci in ER:RAS FSE-hTert cells without 4-OHT treatment (Control), treated with two independent siRNAs against TOP1 (siTOP1-1 and siTOP1-2) and non-targeting siRNA (siCtrl). At least 400 nuclei per condition were analyzed. Data are the summary of two independent experiments. (**d**) Protein levels of TOP1 and GAPDH in ER:RAS FSE-hTert cells with (RAS) or without (Control) 4-OHT treatment and HU and APH treatments as indicated. * $P < 0.05$, ** $P < 0.01$, *** $P < 0.001$.

Supplementary Fig 9. Model for TOP1-dependent accelerated replication and DNA damage. Model of how RAS induces replicative stress generating DNA damage in pre-senescent

cells. RAS activation elevates TOP1 expression, which reduces R-loop levels generating accelerated DNA replication rate progression resulting in DNA damage accumulation.

Supplementary Table 1. Related to Fig. 4. Expression fold change of replication annotated genes. Expression level of replication annotated genes (GO:0006260) and TBP and ISG15, averaged normalized counts and log2 of the fold change are shown.

References

1. Fragkos, M., Ganier, O., Coulombe, P. & Méchali, M. DNA replication origin activation in space and time. *Nat. Rev. Mol. Cell Biol.* **16**, 360–374 (2015).

2. Conti, C. *et al.* Replication Fork Velocities at Adjacent Replication Origins Are Coordinately Modified during DNA Replication in Human Cells. *Mol. Biol. Cell* **18**, 3059–3067 (2007).

3. Ge, X. Q., Jackson, D. A. & Blow, J. J. Dormant origins licensed by excess Mcm2 7 are required for human cells to survive replicative stress. *Genes Dev.* **21**, 3331–3341 (2007).

4. Courbet, S. *et al.* Replication fork movement sets chromatin loop size and origin choice in mammalian cells. *Nature* **455**, 557–560 (2008).

5. Gaillard, H., García-Muse, T. & Aguilera, A. Replication stress and cancer. *Nat. Rev. Cancer* **15**, 276–289 (2015).

6. Zeman, M. K. & Cimprich, K. A. Causes and consequences of replication stress. *Nat. Cell Biol.* **16**, 2–9 (2014).

7. Negrini, S., Gorgoulis, V. G. & Halazonetis, T. D. Genomic instability — an evolving hallmark of cancer. *Nat. Rev. Mol. Cell Biol.* **11**, 220–228 (2010).

8. Hanahan, D. & Weinberg, R. A. Hallmarks of Cancer: The Next Generation. *Cell* **144**, 646–674 (2011).

9. Bartkova, J. *et al.* Oncogene-induced senescence is part of the tumorigenesis barrier imposed by DNA damage checkpoints. *Nature* **444**, 633–637 (2006).

10. Bester, A. C. *et al.* Nucleotide Deficiency Promotes Genomic Instability in Early Stages of Cancer Development. *Cell* **145**, 435–446 (2011).

11. Dominguez-Sola, D. *et al.* Non-transcriptional control of DNA replication by c-Myc. *Nature* **448**, 445–451 (2007).

12. Di Micco, R. *et al.* Oncogene-induced senescence is a DNA damage response triggered by DNA hyper-replication. *Nature* **444**, 638–642 (2006).

13. Galanos, P. *et al.* Chronic p53-independent p21 expression causes genomic instability by deregulating replication licensing. *Nat. Cell Biol.* **18**, 777–789 (2016).

14. Domínguez-Sánchez, M. S., Barroso, S., Gómez-González, B., Luna, R. & Aguilera, A. Genome Instability and Transcription Elongation Impairment in Human Cells Depleted of THO/TREX. *PLoS Genet.* **7**, e1002386 (2011).

15. Bhatia, V. *et al.* BRCA2 prevents R-loop accumulation and associates with TREX-2 mRNA export factor PCID2. *Nature* **511**, 362–365 (2014).

16. Lana, E. *et al.* DNA replication is altered in Immunodeficiency Centromeric instability

Facial anomalies (ICF) cells carrying DNMT3B mutations. *Eur. J. Hum. Genet.* **20**, 1044–1050 (2012).

17. Zhong, Y. *et al.* The level of origin firing inversely affects the rate of replication fork progression. *J. Cell Biol.* **201**, 373–383 (2013).

18. Flach, J. *et al.* Replication stress is a potent driver of functional decline in ageing haematopoietic stem cells. *Nature* **512**, 198–202 (2014).

19. Maya-Mendoza, A. *et al.* High speed of fork progression induces DNA replication stress and genomic instability. *Nature* **559**, 279–284 (2018).

20. Sugimura, K., Takebayashi, S., Taguchi, H., Takeda, S. & Okumura, K. PARP-1 ensures regulation of replication fork progression by homologous recombination on damaged DNA. *J. Cell Biol.* **183**, 1203–1212 (2008).

21. Rimmele, P. *et al.* Spi-1/PU.1 Oncogene Accelerates DNA Replication Fork Elongation and Promotes Genetic Instability in the Absence of DNA Breakage. *Cancer Res.* **70**, 6757–6766 (2010).

22. Raso, M. C. *et al.* Interferon-stimulated gene 15 accelerates replication fork progression inducing chromosomal breakage. *J. Cell Biol.* **219**, (2020).

23. Pylayeva-Gupta, Y., Grabocka, E. & Bar-Sagi, D. RAS oncogenes: weaving a tumorigenic web. *Nat. Rev. Cancer* **11**, 761–774 (2011).

24. Downward, J. Targeting RAS signalling pathways in cancer therapy. *Nat. Rev. Cancer* **3**, 11–22 (2003).

25. Denko, N. C., Giaccia, A. J., Stringer, J. R. & Stambrook, P. J. The human Ha-ras oncogene induces genomic instability in murine fibroblasts within one cell cycle. *Proc. Natl. Acad. Sci. U. S. A.* **91**, 5124–8 (1994).

26. Saavedra, H. I. *et al.* The RAS oncogene induces genomic instability in thyroid PCCL3 cells via the MAPK pathway. *Oncogene* **19**, 3948–54 (2000).

27. Yang, G. *et al.* RAS promotes tumorigenesis through genomic instability induced by imbalanced expression of Aurora-A and BRCA2 in midbody during cytokinesis. *Int. J. Cancer* **133**, 275–285 (2013).

28. Halazonetis, T. D., Gorgoulis, V. G. & Bartek, J. An Oncogene-Induced DNA Damage Model for Cancer Development. *Science (80-.).* **319**, 1352–1355 (2008).

29. Macheret, M. & Halazonetis, T. D. DNA Replication Stress as a Hallmark of Cancer. *Annu. Rev. Pathol. Mech. Dis.* **10**, 425–448 (2015).

30. Ewald, B., Sampath, D. & Plunkett, W. H2AX phosphorylation marks gemcitabine-induced stalled replication forks and their collapse upon S-phase checkpoint abrogation. *Mol. Cancer Ther.* **6**, 1239–1248 (2007).

31. Lukas, C. *et al.* 53BP1 nuclear bodies form around DNA lesions generated by mitotic

transmission of chromosomes under replication stress. *Nat. Cell Biol.* **13**, 243–253 (2011).

32. Glover, T. W., Berger, C., Coyle, J. & Echo, B. DNA polymerase alpha inhibition by aphidicolin induces gaps and breaks at common fragile sites in human chromosomes. *Hum. Genet.* **67**, 136–42 (1984).

33. Miron, K., Golan-Lev, T., Dvir, R., Ben-David, E. & Kerem, B. Oncogenes create a unique landscape of fragile sites. *Nat. Commun.* **6**, 7094 (2015).

34. Skoog, L. & Nordenskjöld, B. Effects of hydroxyurea and 1-beta-D-arabinofuranosyl-cytosine on deoxyribonucleotide pools in mouse embryo cells. *Eur. J. Biochem.* **19**, 81–9 (1971).

35. Técher, H. *et al.* Signaling from Mus81-Eme2-Dependent DNA Damage Elicited by Chk1 Deficiency Modulates Replication Fork Speed and Origin Usage. *Cell Rep.* **14**, 1114–1127 (2016).

36. Ge, X. Q. & Blow, J. J. Chk1 inhibits replication factory activation but allows dormant origin firing in existing factories. *J. Cell Biol.* **191**, 1285–1297 (2010).

37. Koundrioukoff, S. *et al.* Stepwise Activation of the ATR Signaling Pathway upon Increasing Replication Stress Impacts Fragile Site Integrity. *PLoS Genet.* **9**, e1003643 (2013).

38. Cheng, C. H. & Kuchta, R. D. DNA polymerase epsilon: aphidicolin inhibition and the relationship between polymerase and exonuclease activity. *Biochemistry* **32**, 8568–74 (1993).

39. Ikegami, S. *et al.* Aphidicolin prevents mitotic cell division by interfering with the activity of DNA polymerase-alpha. *Nature* **275**, 458–60 (1978).

40. Pommier, Y. Topoisomerase I inhibitors: camptothecins and beyond. *Nat. Rev. Cancer* **6**, 789–802 (2006).

41. Pommier, Y., Sun, Y., Huang, S. N. & Nitiss, J. L. Roles of eukaryotic topoisomerases in transcription, replication and genomic stability. *Nat. Rev. Mol. Cell Biol.* **17**, 703–721 (2016).

42. Tuduri, S. *et al.* Topoisomerase I suppresses genomic instability by preventing interference between replication and transcription. *Nat. Cell Biol.* **11**, 1315–1324 (2009).

43. Santos-Pereira, J. M. & Aguilera, A. R loops: new modulators of genome dynamics and function. *Nat. Rev. Genet.* **16**, 583–597 (2015).

44. Xu, Y. & Her, C. Inhibition of Topoisomerase (DNA) I (TOP1): DNA Damage Repair and Anticancer Therapy. *Biomolecules* **5**, 1652–1670 (2015).

45. Morham, S. G., Kluckman, K. D., Voulomanos, N. & Smithies, O. Targeted disruption of the mouse topoisomerase I gene by camptothecin selection. *Mol. Cell. Biol.* **16**, 6804–9 (1996).

46. Humbert, N. *et al.* A Genetic Screen Identifies Topoisomerase 1 as a Regulator of Senescence. *Cancer Res.* **69**, 4101–4106 (2009).

47. Rømer, M. U. *et al.* TOP1 gene copy numbers in colorectal cancer samples and cell lines and their association to in vitro drug sensitivity. *Scand. J. Gastroenterol.* **47**, 68–79 (2012).

48. Grunnet, M. *et al.* TOP1 gene copy numbers are increased in cancers of the bile duct and pancreas. *Scand. J. Gastroenterol.* **50**, 485–494 (2015).

49. Lee, Y.-C. *et al.* Targeting of Topoisomerase I for Prognoses and Therapeutics of Camptothecin-Resistant Ovarian Cancer. *PLoS One* **10**, e0132579 (2015).

50. Parajuli, S. *et al.* Human ribonuclease H1 resolves R-loops and thereby enables progression of the DNA replication fork. *J. Biol. Chem.* **292**, 15216–15224 (2017).

51. Costantino, L. & Koshland, D. Genome-wide Map of R-Loop-Induced Damage Reveals How a Subset of R-Loops Contributes to Genomic Instability. *Mol. Cell* **71**, 487-497.e3 (2018).

52. Hamperl, S., Bocek, M. J., Saldivar, J. C., Swigut, T. & Cimprich, K. A. Transcription-Replication Conflict Orientation Modulates R-Loop Levels and Activates Distinct DNA Damage Responses. *Cell* **170**, 774-786.e19 (2017).

53. Kotsantis, P. *et al.* Increased global transcription activity as a mechanism of replication stress in cancer. *Nat. Commun.* **7**, 13087 (2016).

54. Das, S. K. *et al.* Poly(ADP-ribose) polymers regulate DNA topoisomerase I (Top1) nuclear dynamics and camptothecin sensitivity in living cells. *Nucleic Acids Res.* **44**, 8363–8375 (2016).

55. Aird, K. M. *et al.* Suppression of Nucleotide Metabolism Underlies the Establishment and Maintenance of Oncogene-Induced Senescence. *Cell Rep.* **3**, 1252–1265 (2013).

56. Maya-Mendoza, A. *et al.* Myc and Ras oncogenes engage different energy metabolism programs and evoke distinct patterns of oxidative and DNA replication stress. *Mol. Oncol.* **9**, 601–616 (2015).

57. Muñoz, S. *et al.* In Vivo DNA Re-replication Elicits Lethal Tissue Dysplasias. *Cell Rep.* **19**, 928–938 (2017).

58. Kunkel, T. A. DNA replication fidelity. *J. Biol. Chem.* **279**, 16895–8 (2004).

59. Sarkisian, C. J. *et al.* Dose-dependent oncogene-induced senescence in vivo and its evasion during mammary tumorigenesis. *Nat. Cell Biol.* **9**, 493–505 (2007).

60. Kim, M. *et al.* Passage-dependent accumulation of somatic mutations in mesenchymal stromal cells during in vitro culture revealed by whole genome sequencing. *Sci. Rep.* **7**, 14508 (2017).

61. Ben-David, U. *et al.* Genetic and transcriptional evolution alters cancer cell line drug

response. *Nature* **560**, 325–330 (2018).

62. Weissbein, U., Benvenisty, N. & Ben-David, U. Genome maintenance in pluripotent stem cells. *J. Cell Biol.* **204**, 153–163 (2014).

63. Bensimon, A. *et al.* Alignment and sensitive detection of DNA by a moving interface. *Science* **265**, 2096–8 (1994).

64. Herrick, J. & Bensimon, A. Single molecule analysis of DNA replication. *Biochimie* **81**, 859–71 (1999).

65. Schindelin, J. *et al.* Fiji: an open-source platform for biological-image analysis. *Nat. Methods* **9**, 676–682 (2012).

66. Greenwood, S. K. *et al.* Population doubling: A simple and more accurate estimation of cell growth suppression in the in vitro assay for chromosomal aberrations that reduces irrelevant positive results. *Environ. Mol. Mutagen.* **43**, 36–44 (2004).

67. Kim, D. *et al.* TopHat2: accurate alignment of transcriptomes in the presence of insertions, deletions and gene fusions. *Genome Biol.* **14**, R36 (2013).

68. Anders, S., Pyl, P. T. & Huber, W. HTSeq--a Python framework to work with high-throughput sequencing data. *Bioinformatics* **31**, 166–169 (2015).

69. Love, M. I., Huber, W. & Anders, S. Moderated estimation of fold change and dispersion for RNA-seq data with DESeq2. *Genome Biol.* **15**, 550 (2014).

70. Wang, J., Duncan, D., Shi, Z. & Zhang, B. WEB-based GEne SeT AnaLysis Toolkit (WebGestalt): update 2013. *Nucleic Acids Res.* **41**, W77–W83 (2013).

Figure 1

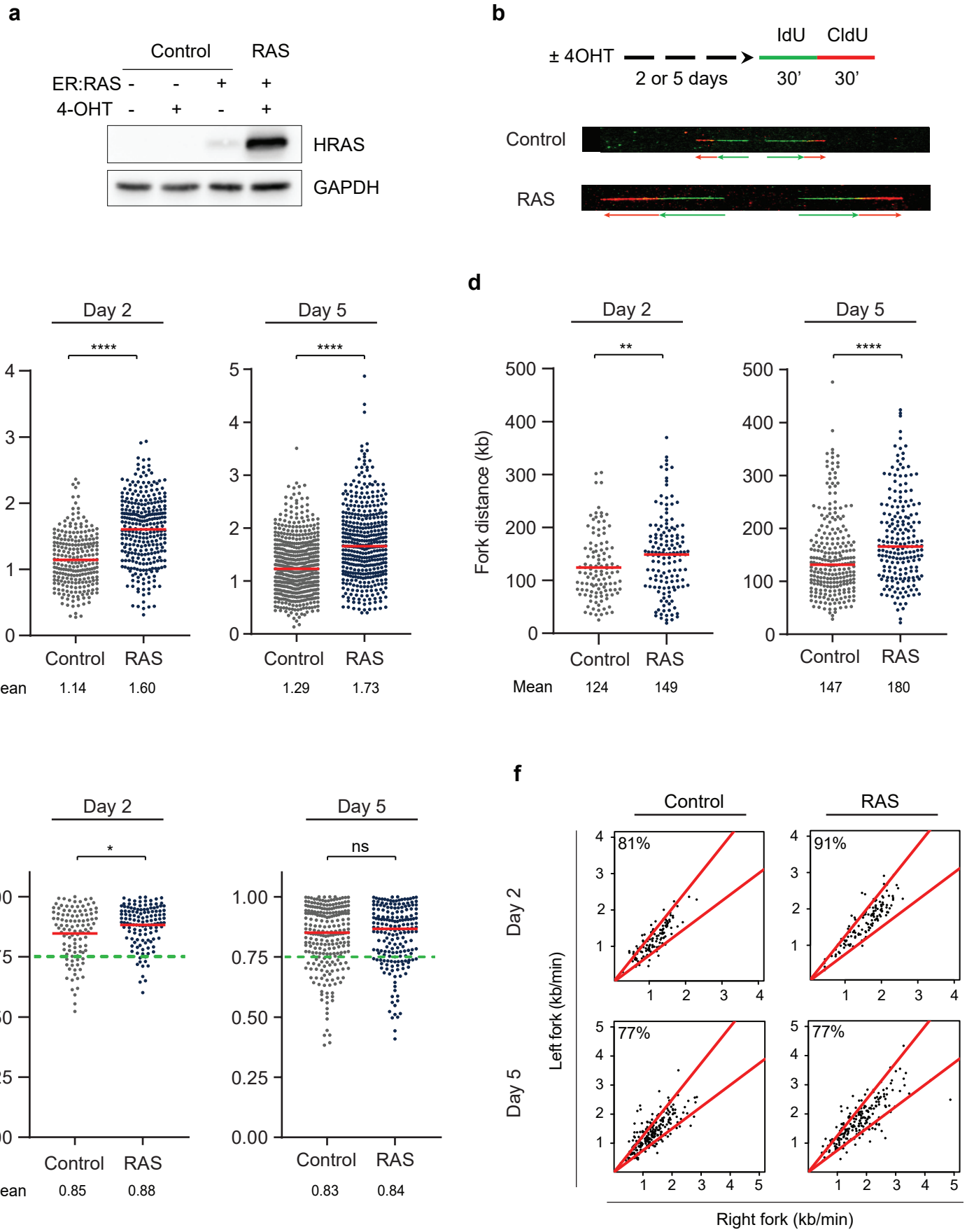

Figure 2

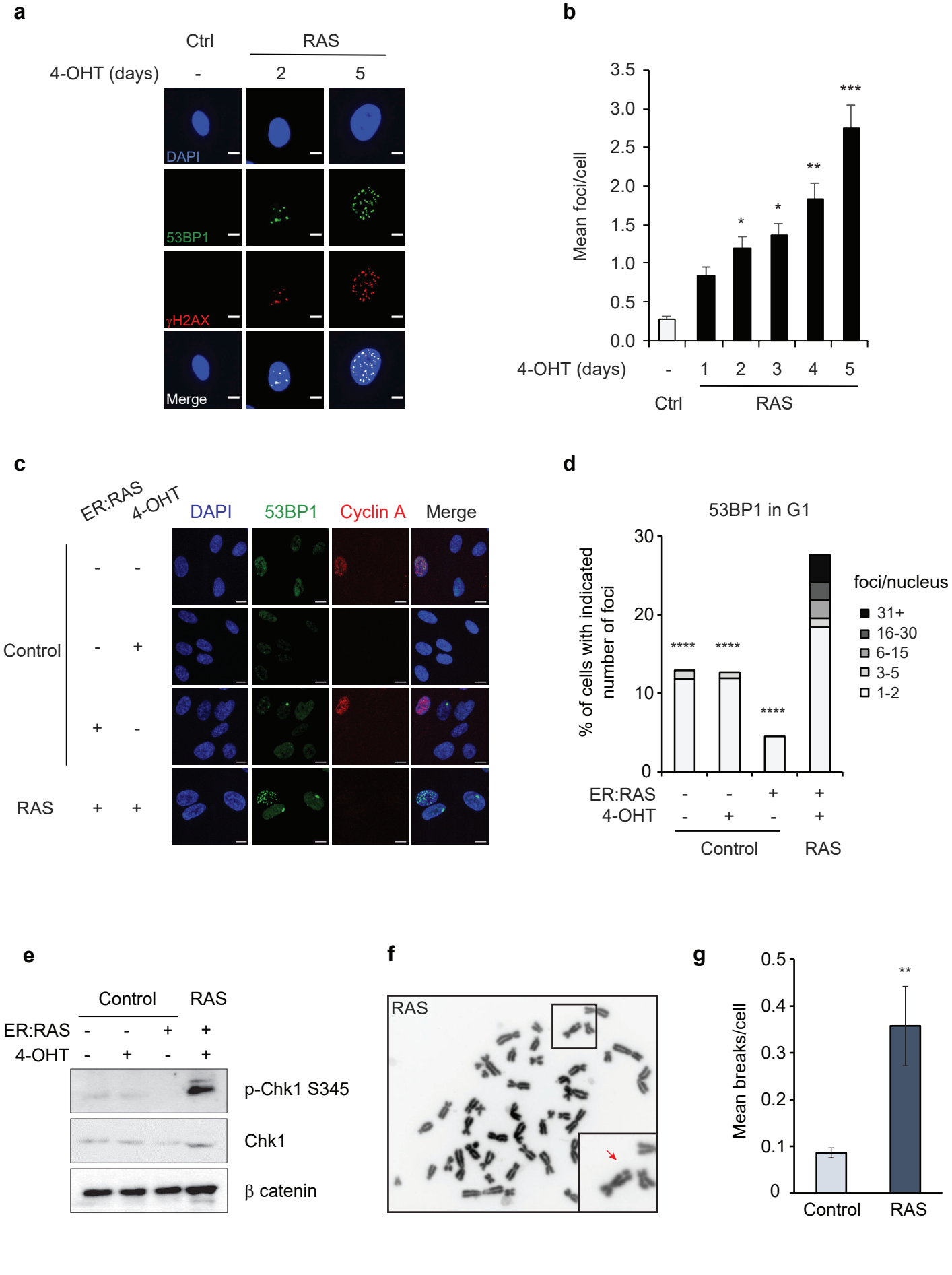

Figure 3

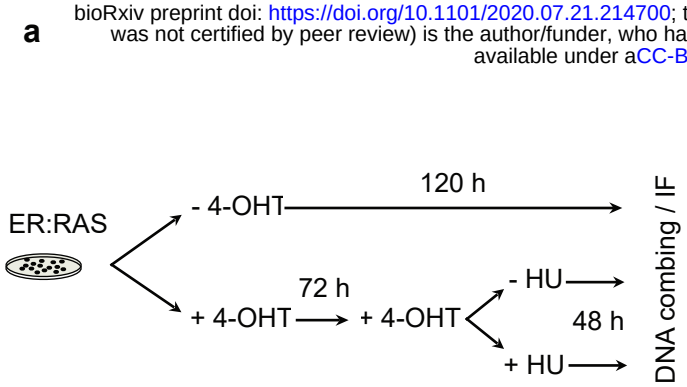

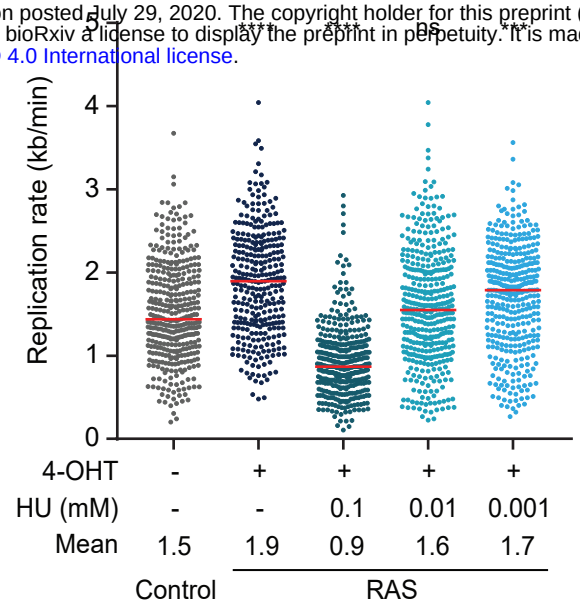

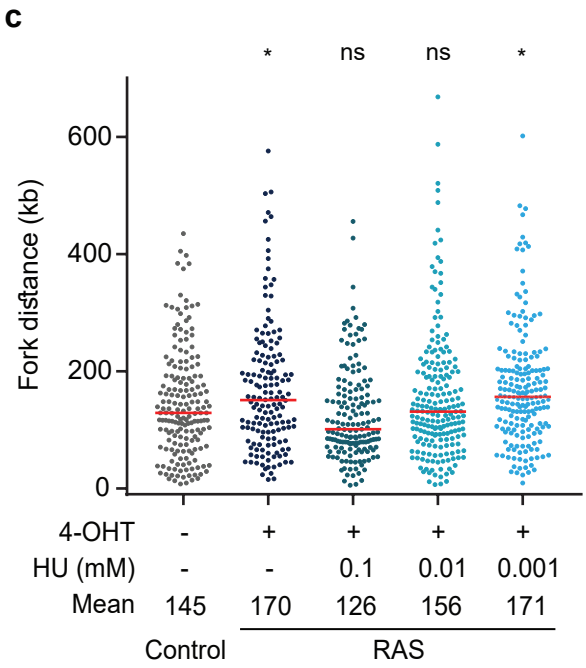

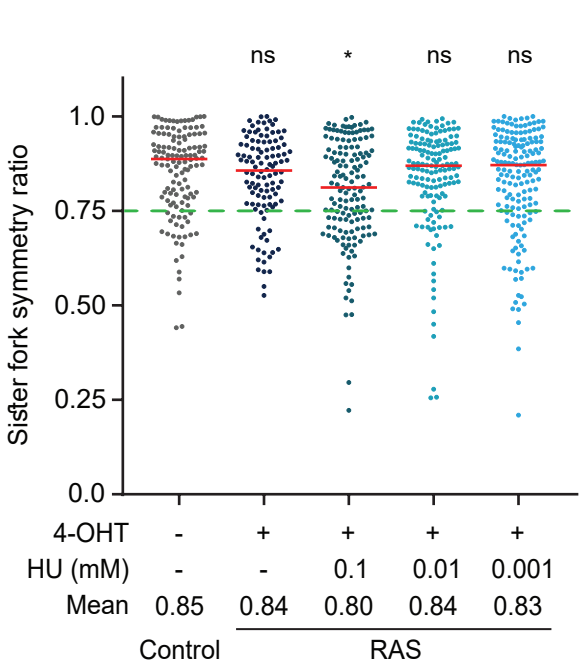

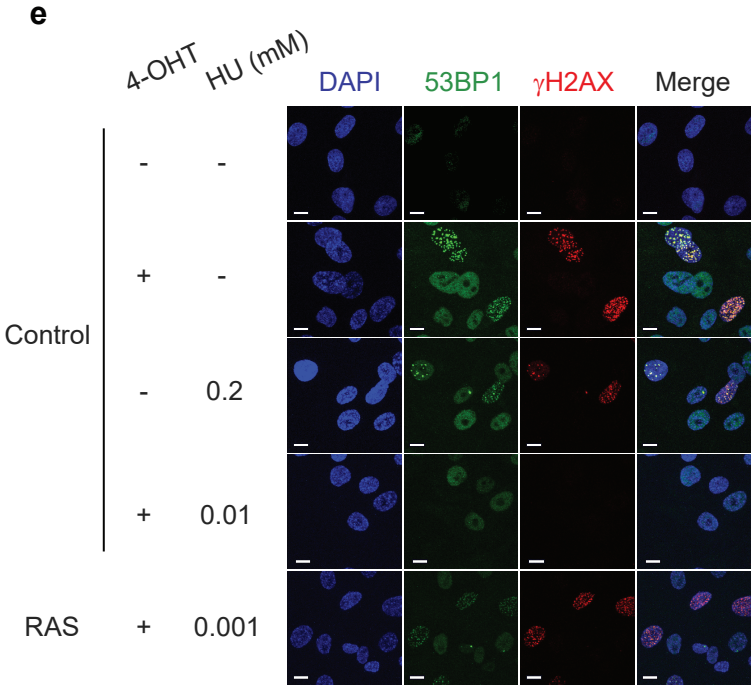

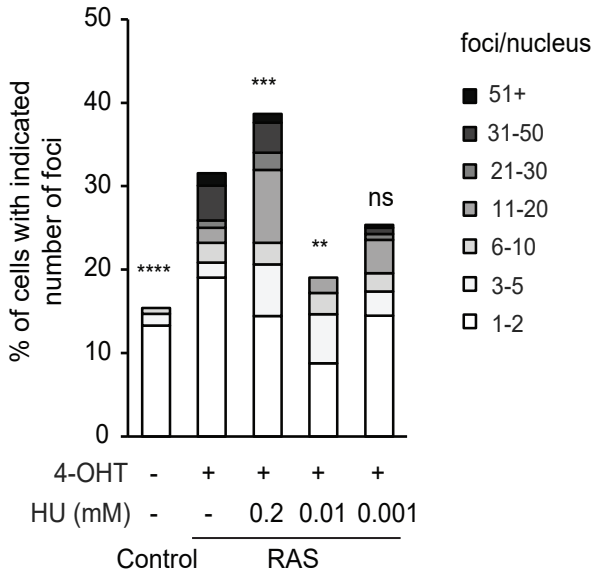

Figure 4

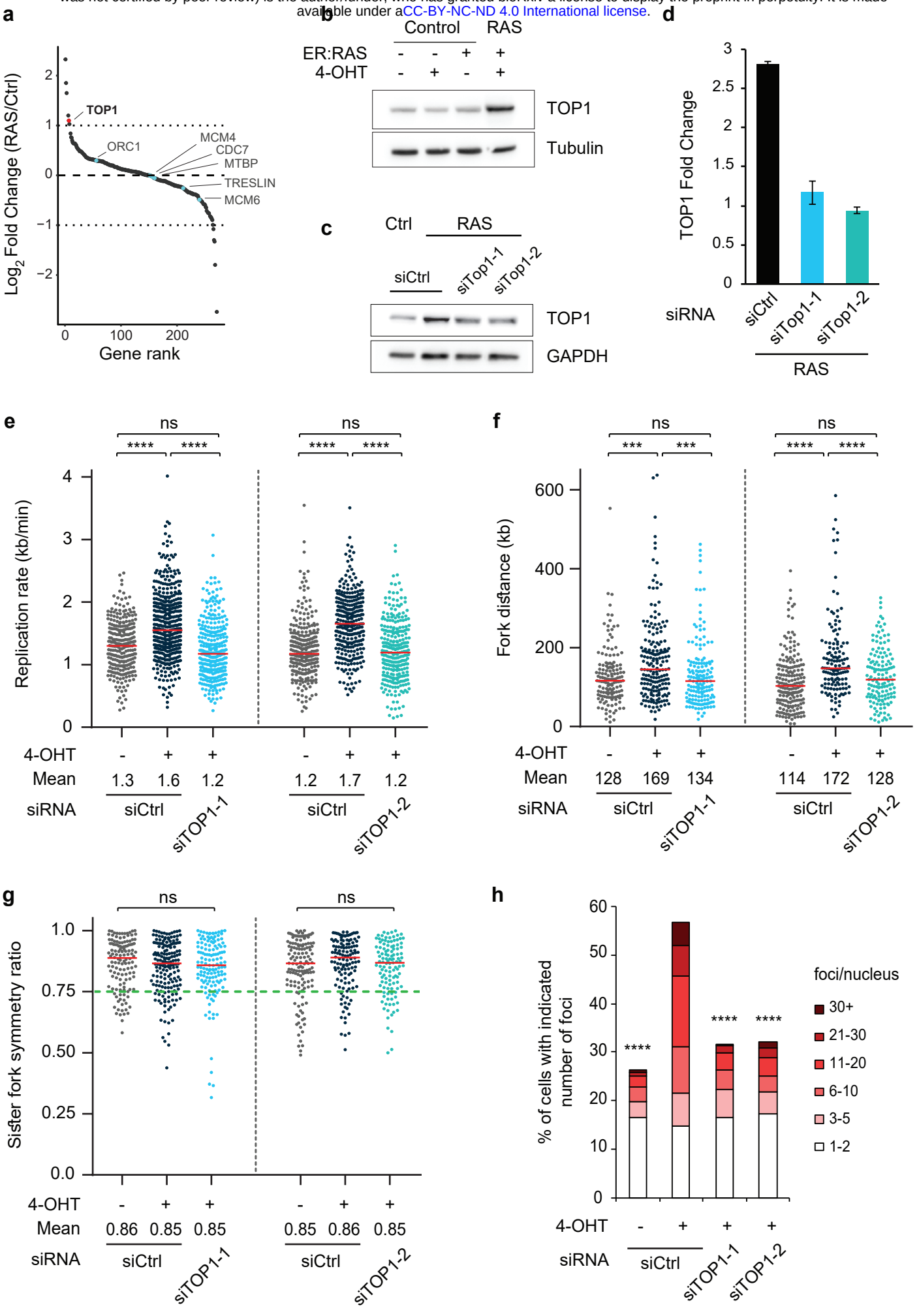

Figure 5

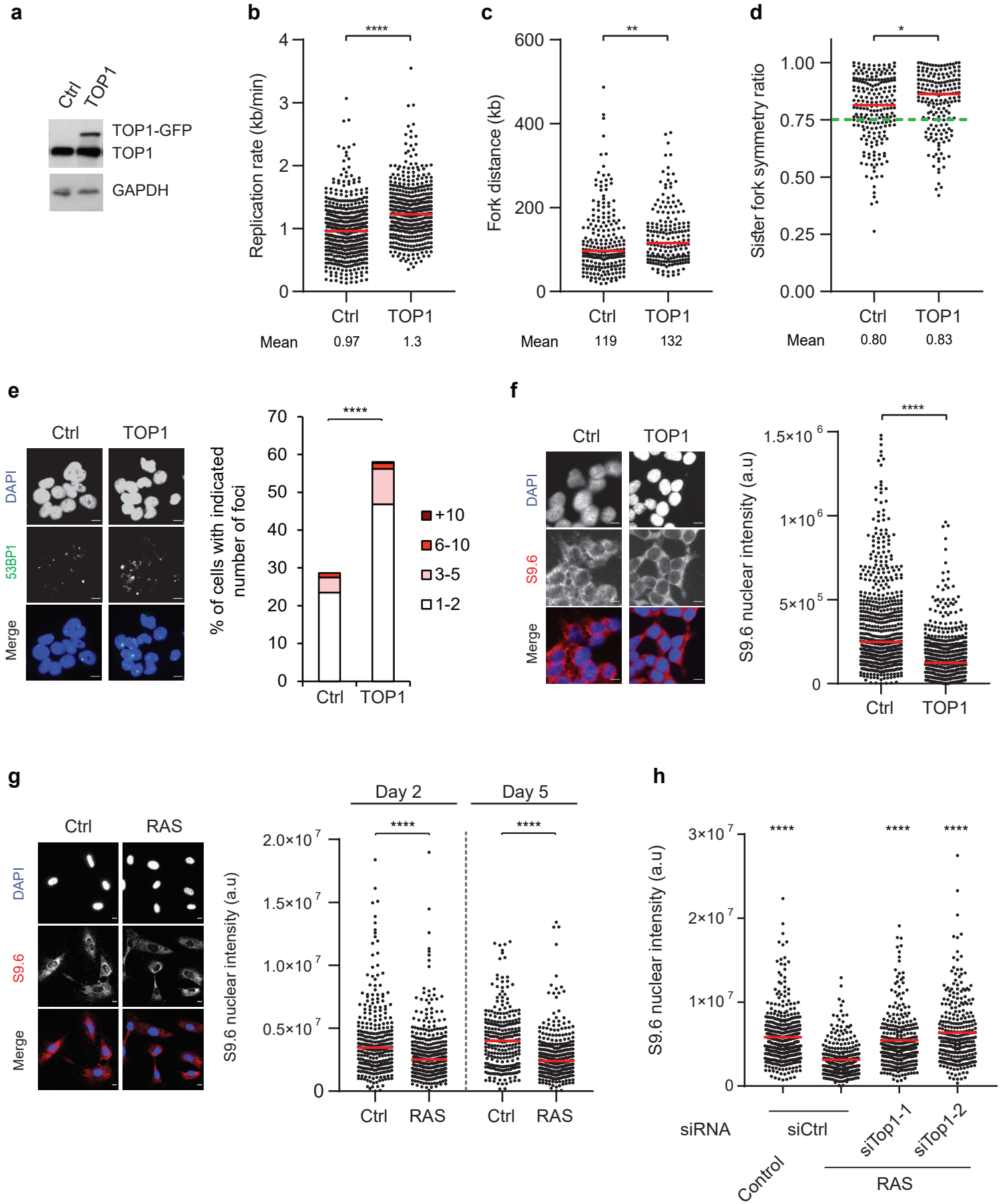

Figure 6